SCALLOP SWIMMING KINEMATICS AND MUSCLE PERFORMANCE: MODELLING THE EFFECTS OF "WITHIN-ANIMAL" VARIATION IN TEMPERATURE SENSITIVITY

DAVID M. BAILEY and IAN A. JOHNSTON

Gatty Marine Laboratory, School of Biology, University of St. Andrews, St. Andrews, Fife, KY16 8LB

Running headline: *Scallop swimming and temperature*

Address for correspondence: D.M. Bailey, Marine Biology Research Division, Scripps Institution of Oceanography, UCSD, 9500 Gilman Drive, La Jolla CA, 92093-0202. E-mail: d4bailey@ucsd.edu, Fax: +1 858 534-7313

Escape behaviour was investigated in Queen scallops (*Aequipecten opercularis*) acclimated to 5, 10 or 15^{o}C and tested at their acclimation temperature. Scallops are active molluscs, able to escape from predators by jet-propelled swimming using a striated muscle working in opposition to an elastic hinge ligament. The first cycle of the escape response was recorded using high-speed video (250 Hz) and whole-animal velocity and acceleration determined. Muscle shortening velocity, force and power output were calculated using a measurements of valve movement and jet area, and a simple biomechanical model. The average shortening speed of the adductor muscle had a Q_{10} of 2.04, significantly reducing the duration of the jetting phase of the cycle with increased temperature. Muscle lengthening velocity and the overall duration of the clap cycle were little changed over the range 5 to 15^{o}C, as these parameters were controlled by the, relatively temperature-insensitive, hinge ligament.

Improvements in the average power output of the adductor muscle over the first clap cycle (222 versus 139 $W \cdot kg^{-1}$ wet mass at 15 and 5°C respectively) were not translated into proportional increases in overall swimming velocity, which was only 32% higher at 15°C (0.37 $m \cdot s^{-1}$) than 5°C (0.28 $m \cdot s^{-1}$).

Keywords: Mollusca, *Aequipecten opercularis*, Swimming, Muscle, Ligament, Temperature

INTRODUCTION

Scallops swim using a form of jet propulsion, the simplicity of which has attracted researchers seeking to study a complete locomotory system. A single adductor muscle, acting in opposition to an elastic hinge ligament powers swimming. When the muscle is activated the shell is pulled closed and water is ejected through jets situated close to the hinge. The animal accelerates forwards (gape first) taking successive "bites" out of the water. The general form of swimming is well described for a number of temperate (Moore and Trueman 1971; Manuel and Dadswell 1990), tropical (Morton 1980; Joll 1989) and polar (Ansell et al. 1998; Bailey et al. in press) species.

Several mechanical aspects of this behaviour have been previously examined including the hydrodynamics of the shells (Thorburn and Gruffydd 1979; Vogel 1985; Milward and Whyte 1991; Anderson et al. 1997), the properties of the hinge ligament (Alexander 1965; DeMont 1988) and the activation of contraction (Stephens and Boyle 1978). The muscle performances involved in scallop swimming have been investigated using *in vitro* muscle preparations (Olson and Marsh 1993; Marsh and Olson 1994), intramantle pressure recordings (Marsh et al. 1992), and mathematical modelling (Cheng et al. 1996; Cheng and Demont 1996b, a, 1997).

Temperature may directly affect the muscle performance of the adductor muscle resulting in changes in fibre shortening velocity *in vitro* (Olson and Marsh 1993), swimming speed (Manuel and Dadswell 1990) and in the form of the clap cycle (Marsh 1990). However the effects of temperature on muscle performance *in vivo* have not been studied and the effect of thermal history on swimming performance is only partially understood (Bailey and Johnston in press). As mechanisms used during the jetting (muscle) and recovery (elastic ligament) phases of scallop swimming differ it is therefore possible that differences in temperature sensitivity will cause differences in the form of the scallop swimming cycle between temperatures.

Environmental temperature has a major effect on locomotory performance and behaviour in many ectothermic animals including lizards (Hertz et al. 1982), frogs (Peplowski and Marsh 1997) and fish (Rome et al. 1990; Beddow et al. 1995; Johnson et al. 1998). Using an integrated approach at different levels of organisation the origins of these changes can sometimes be traced to the effects of temperature on muscle (Wakeling and Johnston 1998; Navas et al. 1999) and enzyme systems (Johnson and Bennett 1995). The relationship between temperature, muscle characteristics and whole-body performance is, however, not straightforward (Bennett et al. 1989; Peplowski and Marsh 1997; Navas et al. 1999).

In the present study swimming behaviour has been analysed during the critical period immediately following first contact between the scallop and its predator. A simple biomechanical model was used to estimate the muscle performances supporting the observed behaviour. Escape responses in animals acclimated to different temperatures were compared in order to investigate changes in the form of the escape response with temperature.

METHODS

Animals

Twenty-four *Aequipecten opercularis* Linnaeus, 1758 (mean shell height 63.6 mm, sd=3.0 mm) were obtained from the University of the Highland and Islands aquaculture facility Ardtoe, Scotland in November 1997. The scallops were allocated to one of 3 groups of 8 animals of the same average body size and acclimated to $5 \pm 0.4^{o}C$, $10 \pm 0.6^{o}C$ and $15 \pm 0.6^{o}C$ (Mean ± range) in temperature controlled recirculating aquaria (Grants Ltd., Cambridge) for 6 weeks. To begin acclimation, tank temperatures were altered in $1^{o}C \cdot day^{-1}$ increments. During acclimation and experimentation the animals were fed *ad libitum* on cultured algae (*Isochrysis galbana*, (Lu and Blake 1996)) and a 12 h light: 12 h dark regime was maintained. The acclimation group to be tested was rotated daily and experiments were completed within 3 weeks of the end of acclimation.

Analysis of Swimming Behaviour

Swimming was filmed in a purpose built tank (80 x 40 x 40 cm, length x width x height) with a mirror mounted above the bottom at 45^{o} to the line of sight of the camera, z' (Fig. 1). The mirror allowed simultaneous top and side views of the tank. Tank temperature was controlled ($\pm 0.2^{o}C$) by a heat exchanger (Grants, Cambridge). A raised glass stage with an attached reference length bar allowed clear views of the scallop during stimulation. A submerged pump and the action of the aeration system ensured that no temperature microclimates existed within the tank. The movement of suspended particles was used to determine ambient water flow ($<0.05\ m.s^{-1}$). Scallop escape responses were recorded on video at 250 Hz (NAC

HSV500c[3], NAC Inc., Japan). The camera was mounted on a tripod 3-4m from the swim tank. A pair of 100 W spotlights illuminated the tank.

24 h before filming 6 points on each scallop (Fig. 1) were marked using 2 mm x 2 mm aluminium foil patches in order to increase the consistency with which those sites were located during digitising. Animals were transferred into the swim tank and allowed to rest for a minimum of 1 h before the first escape response was stimulated by touching the sensory tentacles of the scallop with the tube feet of a dissected starfish (*Asterias rubens*) limb attached to a glass rod. This starfish species is a known predator of *Aequipecten* (Thomas and Gruffydd 1971) and therefore provides an ecologically valid stimulus for eliciting escape responses. There was minimal disturbance of the water around the animal and no force was exerted on the body of the scallop itself. Animals were filmed in rotation with a minimum of 30 min between stimulations (maximum of 5, average of 2.9 stimulations $\cdot$ scallop^{-1} $\cdot$ day^{-1}).

For each stimulation, the animal ID number, tank temperature ($\pm$ 0.1^{0}C), and type of response was recorded. A counter was inscribed onto each frame of the tape during recording. Responses were categorised as "Claps" - animal rapidly closes shell with little or no lateral movement, "Jumps" - animal displaced laterally due to ejection of a jet of water, or "Swims" - animal displaced laterally and vertically making 1 or more claps while above the bottom. Thomas and Gruffydd (1971) described these different types of reaction in detail. Only swims were analysed, due to the high variability (in velocity and direction of movement) of claps and jumps

Morphological Measurements

Following filming, the scallops were dissected and a range of morphological measurements was taken using Vernier callipers (±0.1 mm). Measured and static calculated parameters are shown in Fig. A1 and in the glossary (Table A1). The relationship between each variable and shell height was determined. These were significant ($P < 0.05$, $r^2 > 0.6$, $df = 32$) in all cases.

Analysis of Filming

Video recordings were played frame-by-frame to a PC (Gateway 2000 G6-266) with a video capture board (Hauppauge Win/TV). The co-ordinates of the marked points on both valves were selected by hand and recorded by a purpose-designed package (Visual Basic 4, Microsoft). The spatial resolution of the data was 5 pixels $\cdot$ mm^{-1} (average of 300 pixels $\cdot$ body $length^{-1}$). The magnification possible was determined by the range of movement expected and the screen size available and was close to 1:1. On-screen analysis did not allow parallax error during digitising as the cursor was on the same plane as the point being digitised. Jet areas (*ajet*) during swimming were measured from close-up videos (x4 on-screen magnification) with the animal rotated such that the jet opening was aligned across the film plane (x',y'), (n = 7, representing the entire size range studied).

The co-ordinate data for the first clap cycle following stimulation were analysed in Mathematica (Wolfram Research). A clap cycle started from rest and consisted of the animal closing and then re-opening its shell. For each cycle the animal's shell height, the water temperature and salinity (for calculation of water density) were manually entered into the program. At the start of each cycle a point at the extreme front and rear of the animal and the position of the marked points were digitised with the animal perpendicular to the line of sight

of the camera. The ends of a measured (±0.1 mm) reference bar within the tank were also digitised. Animal orientation was described with reference to an instantaneous co-ordinate system (x,y,z) attached to the animal with the x,z plane the commissural plane of the animal. A fixed system within the tank (x',y'z') described animal position with the film plane of the camera in the x',y' plane (See Fig. 1).

The x' and y' co-ordinates of each marker point were smoothed using moving, piecewise cubic regression in order to remove digitising "noise" from the data. Briefly, this method is analogous to a moving average, but instead a regression was fitted through each section (coordinate 1 to coordinate *n* where *n* is the smooth width) of the data and the mid-point of the curve was recorded as the "smoothed" data point for that section. The procedure was then repeated with the next section of data (coordinate 2 to coordinate *n*+1 etc.)

Whole animal velocity and acceleration in the x' and y' directions was determined by differentiation of smoothed x' and y' co-ordinates of the hinge with respect to time. Resultant velocity (*Ub*) and acceleration (*Xb*) were then calculated.

Smooth width (*n*) was optimised for each sequence independently. The standard error of the raw data around the smoothed positions was calculated for each processed sequence. At the correct *n* this error was similar to that obtained from repeatedly digitising stationary positions on the screen (approximately 0.007 body lengths). Digitising inaccuracies produced apparent rapid changes in gape values; low values of *n* cause a drop in the estimates of work. As *n* increased a plateau was achieved after the removal of digitising errors before *n* became too great and began to cut out "real" data. *n* additional frames were included at the beginning and end of the sequence so that smoothed positions were only calculated from the beginning of the

clap cycle itself. Values of *n* varied between 19 and 23 frames and did not co-vary with animal size, temperature or any swimming performance parameter.

Yaw and roll were defined as rotations about the animal's y and x axes respectively (See Fig 1). Yaw was detected by measuring the projected distance between the hinge and gape marker points in each frame. Yawing may cause velocity and acceleration to be over- or under-estimated depending on the direction of rotation. Velocity and acceleration of the hinge due to rotation of the animal were subtracted from raw values. Sequences in which rotational velocity exceeded 5% of the total measured were not used. Only a small amount of roll (18^{o}) would be required to significantly change (by >5%) the apparent gape recorded, and as roll cannot be quantified from these data all sequences showing roll (e.g. through appearance of the distant edge of the hinge) were not analysed.

Perspective error was minimised by placement of the camera a minimum of 3 m from the swim tank. Initial placement of the animal was within 40 mm of the scale bar. The animal must move 150 mm towards or away from the camera during filming for a 5% difference in measured displacement or gape. As the entire field of view of the camera was limited to 200 mm, this would require the animal to swim at an angle of at least 36.8^{o} from x' (Fig 1). Lens height above the floor was adjusted to match the height of the centre of the field of view, and any remaining error was corrected for by digitising known lengths in the x' and y' directions in the camera's field of view. The resulting aspect ratios were used within the modelling process.

The ability of piecewise moving regression to accurately estimate velocity and acceleration has been assessed by Walker (1998). At the frame rates and magnifications used here this

technique was suitable for the present application. The frame rate used here (250Hz) was close to optimal for the magnification possible (Harper and Blake 1989)

The total net force exerted on the animal by jet thrust and drag (*T*) was calculated from the product of the "virtual mass" of the animal and its tangential acceleration (Daniel 1984). Virtual mass ($Mb_{virtual}$) was the sum of animal wet mass (*Mb*), internal water mass (the weight of water required to fill eviscerated shells minus the volume of the muscle and other tissues) plus the calculated instantaneous volume of the jet cavity; see Appendix A), and the external added mass of water calculated according to the formula for flat discs (Cheng, 1996).

Muscle shortening velocity was calculated from shell gape and the anatomical measurements. The hydrodynamic power output of the jets and muscle force production were estimated from shell gape, jet area, and muscle shortening velocity. A full explanation of the calculations and assumptions can be found in Appendix A.

RESULTS

Biomechanics Of Swimming In Animals Acclimated To Different Temperatures

Clap cycles consisted of a short period of rapid shell closing (adduction), reducing in rate until reaching zero velocity, after which re-opening was rapid and returned the gape to the length prior to the beginning of the cycle. Temperature strongly affected the first clap cycle during simulated escape responses in animals swimming at their acclimation temperature. At higher temperatures shell closure was completed earlier without an apparent change in the rate of reopening. This resulted in differences in both the form (Fig. 2A) and duration (0.53s at 5^{o}C to 0.30s at 15^{o}C, r^2=0.95, $p<0.001$, df=23) of the clap cycle.

Measurements of the animal's acceleration (*Xb*) and the virtual mass of the animal, $Mb_{virtual}$, (including associated water) allowed the net force (*T*, N) on the animal caused by the jet impulse to be calculated (Fig. 2B). During initial closing thrust exceeded drag and the animal accelerated forwards until, nearing shell closure, thrust was approximately equal to drag. On re-opening of the valves rapid deceleration resulted from the increased drag experienced by the animal and the cessation of any remaining impulse from the jets. *Tmax* was significantly higher at 15°C (1.15 N) than at 5°C (0.61 N) and was attained earlier in the cycle (Fig. 2B, Table 1).

Swimming velocity (*Ub*) increased rapidly during shell closure, reaching a maximum at approximately 5% of maximum gape (Fig. 2C). *Ub* reduced slowly as jetting ended and then fell rapidly on valve opening. Increased thrust (*T*) at higher temperatures resulted in increased mean swimming velocity during jetting, $\bar{U}b_{jet}$, (Table 2) with maximum velocity, *Ubmax*, attained earlier in the cycle than at lower temperatures (Fig. 2C). The Q_{10} of Ub_{jet} was higher than that for $\bar{U}b$ or *Ubmax* (Table 2) although *Ubmax* did significantly increase from 0.28 m · s^{-1} at 5^0C to 0.37 m · s^{-1} at 15°C (Table 1 and 2).

The modelling of muscle performance during the escape responses described above revealed the underlying changes in muscle properties involved. Instantaneous muscle length (*Lm*) was calculated from the gape of the shell (Fig. 2A) and detailed anatomical measurements (Appendix A). Fibre shortening velocity ($\hat{U}m$) rose rapidly then fell throughout closure (Fig. 3). Lengthening was more rapid and reached a maximum after around 0.07s of reopening (at all test temperatures). $\hat{U}m$ then fell until the end of the cycle. Mean muscle shortening

velocity during jetting increased with increasing temperature while muscle lengthening velocity did not (Table 1 and 2).

Power output (*P*) and force production (*F*) were calculated from the shortening velocity of the muscle, the jet area (*ajet*) and flow rate (*f*) of water through the jets (see Appendix A). Tension (F_{spec}), was calculated from the resting cross-sectional area of the adductor (*am*). Predicted workloops (F_{spec}, against muscle strain, *S*) and tension-velocity (F_{spec} vs. $\hat{U}m$) trajectories were plotted from the model output (Fig. 4A and B). Strains were calculated relative to the maximum muscle length, immediately prior to shortening. Workloops showed a rapid increase in F_{spec} with decreasing muscle length reaching a maximum tension at approximately 90% of starting length. F_{spec} fell sharply then continued to fall more slowly to zero with a shortening of around 20%. Lengthening was associated with a small negative force requirement to open the valves. This force fell during lengthening. *Fmax* occurred at slightly greater fibre length at 5^{o}C than at the other two temperatures.

During shortening force-velocity trajectories fitted to a quadratic function (r^2=0.998, p<0.001, df=34, $F_{spec} = 29.872 \cdot \hat{U}m^2 + 7.0347x + 2.3295$) with *Fmax* occurring simultaneously with maximum shortening velocity, $\hat{U}mmax$, (Fig. 4). As force development and velocity are directly interdependent in this locomotory system the forces during increases and decreases in velocity are overlaid. During lengthening (positive values) F_{spec} is low due to the large area through which the flow into the mantle occurs. This negative force requirement is reduced as the shell opens due to the increasing area of gape. The shape of the predicted force-velocity trajectories did not differ with temperature although the length of the trajectory depended on $\hat{U}mmax$.

Power output (P) increased to a maximum (P_{max}) almost immediately upon the commencement of adduction with a rapid fall in power output as shortening velocity fell. The power production was completed earlier at higher temperature. A small negative power requirement was observed beginning at the start of valve opening. Only mean cyclic power output, $\bar{P}_{spec}$, and mean tension, $\bar{F}_{spec}$, were significantly related to temperature due to the high variance of *Pmax* and *Fmax* (Table 1). $\bar{P}_{spec}$ increased from 11.7 to 31.1 $W \cdot kg^{-1}$ and $\bar{F}_{spec}$ from 12.5 to 28.8 $kN \cdot m^{-2}$ as temperature increased from 5 to 15^{o}C. In general muscle performance was higher and jetting completed sooner at higher temperatures.

DISCUSSION

Effects Of Temperature On Swimming

Aequipecten opercularis is a species for which temperature variation over daily and seasonal timescales is an important environmental feature. Given the known importance of swimming to the ecology of scallops it is surprising that the effects of temperature on scallop swimming have not attracted more attention.

Our data show that when animals were stimulated to swim at their acclimation temperature whole-body performance was strongly temperature-dependent, with warmer animals swimming faster, leaving the bottom sooner and with higher accelerations than animals at lower temperatures. These changes in whole-body performance were associated with a reduction in the time spent shortening the adductor and a resultant decrease in clap period. Our data show that over the range of 5-15^{o}C the time taken for shell closure fell by 57%, while the time taken to re-open the shell fell by only 31%. As a result the overall change in clap

period was a decrease of 48% from 5 to 15^{o}C. These changes in shell movement resulted in significant increases in all whole-body measures of performance with higher acclimation temperature. Similarly, all measures of muscle performance increased with temperature except muscle lengthening velocity. Here though, many relationships were non-significant due to individual variability in the data.

Few other detailed studies of the effects of temperature on scallop swimming or muscle performance exist. Bailey and Johnston (in press) have previously demonstrated that temperature acclimation in the field modified various swimming parameters in *A. opercularis*, maintaining escape performance at lower temperatures. Peck and co-workers (2004) recently showed how higher temperatures (1-2^{o}C) disable Antarctic scallops, and other invertebrates by depriving them of the aerobic scope required for locomotion and/or muscular recovery.

The only other study using high-speed recordings at different temperatures was reported by Marsh (1990) in *Argopecten irradians* at 10 and 20^{o}C, who concluded that clap frequency was controlled by the time from the end of shortening to the beginning of lengthening, with little modification to either the opening or closing phases with temperature. In contrast, video recordings of *Placopecten magellanicus* made by Dadswell and Weihs (1990) indicated a shortening of the power stroke with increasing temperature with muscle shortening velocity increasing by 50% as temperature increased from 3.4 to 11.2^{o}C. Direct effects of temperature on muscle characteristics appear to be important in mediating the influence of temperature on scallop swimming. *In vitro* experiments on the muscle fibres of acclimated scallops (*Argopecten irradians*) by Olson and Marsh (1993) showed elevated intrinsic shortening velocity with increasing temperature and higher force production for a given shortening velocity i.e. a change in the shape of the force-velocity relationship. In contrast, the

experiments presented here show little change in the form of the workloops and force-velocity trajectories obtained for the adductor muscle at different temperatures. Temperature acted upon the shortening velocity of the muscle changing the position on the force-velocity curve but did not alter the shape of the relationship. This resulted in maximum tension being produced at greater muscle length in cold-acclimated (5^{o}C) than warm-acclimated (15^{o}C) animals. The form of the force-velocity trajectory was fixed by the relationship between shortening velocity and flow for an individual animal. This relationship depends on the plane area of the mantle cavity and the areas through which water entered or left the shell (*ajet*). The difficulty of accurately measuring the *ajet* is a significant limitation to the method of estimating jet characteristics used here. In this regard our method is similar to that of Cheng and Demont (1997). Interestingly the transient peaks in force and power that have been observed during *in vitro* workloops (Marsh and Olson 1994) and pressure-flow experiments (Marsh et al. 1992) are absent from both the present study and that of Cheng and Demont (1997). It is possible that the absence of such peaks may be a result of our incomplete understanding of mantle behaviour during early jetting.

"Within-Animal" Variation In Temperature Sensitivity?

The kinematic studies presented here show differences in temperature dependence between the opening and closing phases of scallop swimming, and these differences have effects on estimates of muscle performance for animals at different temperatures. Scallops lack the antagonistic muscle systems used by most animals, relying instead on an elastic ligament and flow around the shell to reopen the shell and stretch the adductor (Vogel 1985). In the present study these forces appear to be relatively temperature insensitive compared to the adductor muscle,

Temperature is likely to have a particularly powerful effect on scallop muscle *in vivo* as these animals have no ability to gear muscle use (e.g to utilise less fibres at higher temperatures) as the entire fast muscle is activated simultaneously during contraction (Marsh et al. 1992). Similarly there is little opportunity to change the timing of fast muscle activation as cyclical contractions are triggered when the hinge ligament stretches the muscle (Mellon 1968). Once escape swimming has begun the locomotory system is a cyclical pump, the performance of which is not controlled by fast muscle innervation. The modulation of shortening velocity and force production by the adductor then depends on the cross-sectional area of the jet. This is an unusual case where muscle and swimming performance are under the neurological control of a muscle system which itself does little or none of the actual work. A further unusual feature of scallop locomotion is the marked temporal separation of the temperature sensitive and temperature independent phases of the locomotory cycle, resulting in the observed changes in the form of the escape swimming in scallops at different temperatures.

Acknowledgements

This work was carried out as part of a NERC CASE studentship supervised by IAJ and Prof. Lloyd Peck (British Antarctic Survey). The help and advice of Dr. J. Wakeling during the development of the model, and the comments of the reviewers are gratefully acknowledged. The image analysis software used was written and provided by Dr. B. Batty. Mr. Adrian Walker and the EPSRC Engineering Instrument Pool provided the excellent high-speed video equipment, and training in its use.

References

Alexander, R.M. (1965). Rubber-like properties of the inner hinge-ligament of the pectinidae. *J. Exp. Biol.*, **44,** 119-130.

Anderson, E.J., MacGillivray, P.S. and DeMont, M.E. (1997). Scallop shells exhibit optimization of riblet dimensions for drag reduction. *Biol. Bull.*, **192,** 341-344.

Ansell, A.D., Cattaneo-Vietti, R. and Chiantore, M. (1998). Swimming in the Antarctic scallop *Adamussium colbecki*: analysis of *in situ* video recordings. *Antarct. Sci.*, **10,** 369-375.

Bailey, D.M. and Johnston, I.A. (in press). Temperature acclimatisation of muscle performance in the European Queen Scallop. *J. Therm. Biol.*

Bailey, D.M., Johnston, I.A. and Peck, L.S. (in press). Invertebrate muscle performance at high latitude: swimming activity in the Antarctic scallop, *Adamussium colbecki*. *Polar Biol.*

Beddow, T.A., van Leeuwen, J.L. and Johnston, I.A. (1995). Swimming kinematics of fast starts are altered by temperature acclimation in the marine fish *Myoxocephalus scorpius*. *J. Exp. Biol.*, **198,** 203-208.

Bennett, A.F., Garland, T., Jr. and Else, P.L. (1989). Individual correlation of morphology, muscle mechanics, and locomotion in a salamander. *Am. J. Physiol.*, **256,** R1200-8.

Cheng, J.-Y., Davison, I.G. and Demont, M.E. (1996). Dynamics and energetics of scallop locomotion. *J. Exp. Biol.*, **199,** 1931-1946.

Cheng, J.-Y. and Demont, M.E. (1996a). Hydrodynamics of Scallop Locomotion - Unsteady Fluid Forces On Clapping Shells. *J. Fluid Mech.*, **317,** 73-90.

Cheng, J.-Y. and Demont, M.E. (1996b). Jet-propelled swimming in scallops: Swimming mechanics and ontogenic scaling. *Can. J. Zool.*, **74,** 1734-1748.

Cheng, J.-Y. and Demont, M.E. (1997). A predicted in vivo muscle force - Velocity trajectory. *Can. J. Zool.*, **75,** 371-375.

Dadswell, M.J. and Weihs, D. (1990). Size-related hydrodynamic characteristics of the giant scallop, *Placopecten magellanicus* (Bivalvia: Pectinidae). *Can. J. Zool.*, **68,** 778-785.

Daniel, T.L. (1984). Unsteady aspects of aquatic locomotion. *Am. Zoo.*, **24,** 121-134.

DeMont, M.E. (1988). Tuned oscillations in the swimming scallop *Pecten maximus*. *Can. J. Zool.*, **68,** 786-791.

Harper, D.G. and Blake, R.W. (1989). A critical analysis of the use of high-speed film to determine maximum accelerations of fish. *J. Exp. Biol.*, **142,** 465-471.

Hertz, P.E., Huey, R.B. and Nevo, E. (1982). Fight versus flight: body temperature influences defensive responses of lizards. *Anim. Behav.*, **30,** 676-679.

Johnson, T.P. and Bennett, A.F. (1995). The thermal acclimation of burst escape response in fish: an integrated study of molecular and cellular physiology and organismal performance. *J. Exp. Biol.*, **198,** 2165-2175.

Johnson, T.P., Cullum, A.J. and Bennett, A.F. (1998). Partitioning the effects of temperature and kinematic viscocity on the c-start performance of adult fishes. *J. Exp. Biol.*, **201,** 2045-2051.

Joll, L.M. (1989). Swimming behaviour of the saucer scallop *Amusium balloti* (Mollusca: Pectinidae). *Mar. Biol.*, **102,** 299-305.

Lu, Y.T. and Blake, N.J. (1996). Optimum concentrations of Isochrysis galbana for growth of larval and juvenile bay scallops, *Argopecten irradians concentricus* (Say). *J. Shellfish Res.*, **15,** 635-643.

Manuel, J.L. and Dadswell, M.J. (1990). Swimming behaviour of juvenile giant scallop, *Placopecten magellanicus,*in relation to size and temperature. *Can. J. Zool.*, **69,** 2250-2254.

Marsh, R.L. (1990). Deactivation rate and shortening velocity as determinants of contractile frequency. *Am. J. Physiol.*, **259,** R223-R230.

Marsh, R.L. and Olson, J.M. (1994). Power output of scallop adductor muscle during contractions replicating the in vivo mechanical cycle. *J. Exp. Biol.*, **193,** 139-56.

Marsh, R.L., Olson, J.M. and Guzik, S.K. (1992). Mechanical performance of scallop adductor muscle during swimming. *Nature*, **357,** 411-3.

Mellon, D., Jr. (1968). Junctional physiology and motor nerve distribution in the fast adductor muscle of the scallop. *Science*, **160,** 1018-20.

Milward, A. and Whyte, M.A. (1991). The hydrodynamic characteristics of six scallops of the Super Family Pectinacea, Class Bivalvia. *J. Zool.*, **227,** 547-566.

Moore, J.D. and Trueman, E.R. (1971). Swimming of the scallop, *Chlamys opercularis* (L.). *J. Exp. Mar. Biol. Ecol.*, **6,** 179-185.

Morton, B. (1980). Swimming in *Amusium pleuronectes* (Bivalvia: Pectinidae). *J. Zool.*, **190,** 375-404.

Navas, C.A., James, R.S., Wakeling, J.M., Kemp, K.M. and Johnston, I.A. (1999). An integrative study of the temperature dependence of whole animal and muscle performance during jumping and swimming in the frog *Rana temporaria*. *J. Comp. Phys. - B*, **169,** 588-96.

Olson, J.M. and Marsh, R.L. (1993). Contractile properties of the striated adductor muscle in the bay scallop *Argopecten irradians* at several temperatures. *J. Exp. Biol.*, **176,** 175-93.

Peck, L.S., Webb, K.E. and Bailey, D.M. (2004). Extreme sensitivity of biological function to temperature in Antarctic marine species. *Func. Ecol.*, **18,** 625-630.

Peplowski, M.M. and Marsh, R.L. (1997). Work and power output in the hindlimb muscles of Cuban tree frogs *Osteopilus septentrionalis* during jumping. *J. Exp. Biol.*, **200,** 2861-2870.

Podolsky, R.D. and Emlet, R.B. (1993). Separating the effects of temperature and viscocity on swimming and water movement by sand dollar larvae (*Dendraster excentricus*). *J. Exp. Biol.*, **176,** 207-221.

Rome, L.C., Funke, R.P. and Alexander, R.M. (1990). The influence of temperature on muscle velocity and sustained performance in swimming carp. *J. Exp. Biol.,* **154,** 163-78.

Stephens, P.J. and Boyle, P.R. (1978). Escape responses of the Queen Scallop *Chlamys opercularis* (L.) (Mollusca: Bivalvia). *Mar. Behav. Physiol.*, **5**

Thomas, G.E. and Gruffydd, L.D. (1971). The types of escape reactions elicited in the scallop *Pecten maximus* by selected sea-star species. *Mar. Biol.*, **10,** 87-93.

Thorburn, I.W. and Gruffydd, L.D. (1979). Studies of the behaviour of the scallop *Chlamys opercularis* (L.) and its shell in flowing sea water. *J. Mar. Biol. Assoc. UK.*, **59**

Vogel, S. (1985). Flow-assisted shell reopening in swimming scallops. *Biol. Bull.*, **169,** 624-630.

Wakeling, J.M. and Johnston, I.A. (1998). Muscle power output limits fast-start performance in fish. *J. Exp. Biol.*, **201,** 1505-1526.

Walker, J.A. (1998). Estimating velocities and accelerations of animal locomotion: A simulation experiment comparing numerical differentiation algorithms. *J. Exp. Biol.*, **201,** 981-995.

Weihs, D. (1980). Energetic significance of changes in swimming modes during growth of larval Anchovy, *Engraulis mordax*. *Fish. Bull.*, **77,** 597-604.

Appendix A,

MODELLING SCALLOP SWIMMING

A simple model of scallop swimming was constructed which used the detailed morphological measurements and high-speed video sequences of take-off behaviour to estimate muscle performance. Briefly, the change in volume of water within the shell during clapping (flow, *f*) and the jet cross-sectional area (*ajet*) were used to calculate jet mass and velocity. From this jet power output was determined, and with knowledge of muscle shortening velocity (*Um*) force production (*F*) could also be calculated.

Assumptions

The mathematical model assumed that the shell valves are rigid, and pivoted only at the hinge, and therefore do not change in internal volume. Digitised silhouettes of scallops during swimming showed no change in lateral section area other than that of the mantle cavity. It was not possible to determine whether or not the shell was deformed laterally (i.e. gets wider or narrower). Water was assumed to be inviscid and incompressible at the pressures involved in this study. At the water temperatures, salinities, swimming velocities, and animal sizes (See Methods and Results sections) involved here Re>10,000. Experiments in fish have demonstrated that the effects of temperature on viscosity are insignificant compared to its effects on physiology for anything bigger than larvae and early juvenile fish (Weihs 1980; Podolsky and Emlet 1993; Johnson et al. 1998)

Over 99% of the work done by the adductor muscle goes to power the jets (Cheng et al. 1996), the power output of which was determined in a similar way in the present study. The error caused by not modelling the complete hydrodynamics of the scallop is therefore small.

Calculation of Muscle Length

The gape angle (*Ag*) was calculated from the distance between the digitised points (Lg_{points}) on the valve edges and their distance from the hinge (Lsh_{points}), Fig. A1). The distance from the points to the hinge was measured in the first shot of the sequence and remains the same throughout. The angles between the centreline and the muscle scars were calculated from the depth of the valves (Lsd_t and Lsd_b) and the distances from the scars to the hinge parallel to the centreline. These measurements gave the internal top and bottom angles, Ai_t and Ai_b, and remain constant throughout. The sum of these angles was then the angle over which the muscle was extended (*Amext*).

$$Amext = A_g + Ai_t + Ai_b$$
$$= 2ArcSin\left(\frac{Lg_{po\,int\,s}}{2Lsh_{po\,int\,s}}\right) + ArcTan\left(\frac{Lsd_t}{Lsh - Lmf_t}\right) + ArcTan\left(\frac{Lsd_b}{Lsh - Lmf_b}\right)$$

Muscle length was calculated by considering the two valves separately in order to keep the geometry relatively simple. Muscle length above the centreline was calculated from angle Ai_t + the angle from the commissural plane to the valve edge (equal to half the gape angle *Ag*), and the direct distance between muscle scar and hinge (*Lmh*). The length of the lower portion of the muscle was calculated in the same way and the two summed to give the total muscle length, Lm_v.

$$Lmh_t = \sqrt{Lsd_t{}^2 + (Lsh - Lmf_t)^2}$$

$$Lmh_b = \sqrt{Lsd_b{}^2 + (Lsh - Lmf_b)^2}$$

$$Lm_v = Sin\left(\left(\frac{Ag}{2}\right) + Ai_t\right) \cdot Lmh_t + Sin\left(\left(\frac{Ag}{2}\right) + Ai_b\right) \cdot Lmh_b$$

The adductor muscle may be obliquely positioned within the shell, both laterally and front to rear. The lateral displacement (*Lmm*) was measured upon dissection and used to calculate a corrected muscle length where the length taking into account lateral displacement was the hypotenuse, and the uncorrected length and lateral displacement the known two sides of a triangle (Fig. A1).

$$Lm_{lat} = \sqrt{M_v{}^2 + Lmm^2}$$

The front to rear displacement *(Lm_{anti})* was variable due to the rotation of the shells during movement. This displacement was maximal at Gape (*Lg*)=zero and equal to the horizontal difference between the two muscle scars. This displacement was reduced as gape increases until at *Lg*=180 degrees the displacement would be zero as the scars would be above each other. The front to rear displacement parallel to the commissural (x,z) plane is needed to calculate muscle length where the actual muscle length (*Lm*) was the hypotenuse and the front to rear displacement (Lm_{anti}) and previously calculated length (Lm_{lat}) were the known sides (Fig. A1).

$$Lm_{anti} = Cos\left(\left(\frac{Ag}{2}\right) + Ai_t\right) \cdot Lmh_t - Cos\left(\left(\frac{Ag}{2}\right) + Ai_b\right) \cdot Lmh_b$$

$$Lm = \sqrt{Lm_{lat}{}^2 + Lm_{anti}{}^2}$$

Jet Characteristics

A scaling formula was generated which relates shell height to maximum jet area (see Table A1); this may slightly under estimate jet performance late in the cycle but gives realistic values for the maximum muscle performance. Cheng and Demont (1996b) used mean jet area in their calculations and possibly overestimate maximum performance as a result. The circumference (*Lc*) of the projected shell area (as_{proj}), the length of the arc blocked by the hinge (Lh_{arc}) and gape were used to calculate the gape area through which water enters the shell on re-opening, *ag*.

$$ag = \left(Lc - Lh_{arc}\right) \cdot \left(\frac{Lg}{2}\right)$$

Jet cavity volume (*vc*) was calculated from the projection of the elliptical plane area of the valves onto the commissural (x,y) plane where Lsh_{proj} is the scallop's shell height projected onto the commissural plane.

$$Lsh_{proj} = \sqrt{Lsh^2 - \left(\frac{Lg}{2}\right)^2}$$

$$vc = \left(\frac{\pi \cdot Lsh_{proj} \cdot Lsl \cdot Lg}{2}\right)$$

Flow (*f*) was calculated from the cavity volume data by differentiating a moving cubic regression of cavity volume against time. Jet velocity (*Ujet*) was calculated by dividing flow by jet area (*ajet*). Intake velocity (*Uin*) was calculated by dividing flow by gape area (*ag*). Changes in the sign of the flow term were used to trigger the change from output through the vent to intake through the gape.

$$Uin = \frac{f}{ag}$$

$$Ujet = \frac{f}{ajet}$$

Hydrodynamic power (*P*) was calculated from flow (*f*), jet or intake water velocity (*Ujet* or *Uin* respectively) and seawater density at the experimental temperature (ρ). *Ujet* was used in the formula below, where *Uin* was used to calculate power required during opening. Dividing by adductor wet mass (*Mm*) yielded muscle mass specific power output (*Pspec*).

$$P_{Spec} = \frac{\left(\frac{1}{2} f.\rho.Ujet^2\right)}{M_m}$$

Muscle Area Specific Force Development

Muscle shortening velocity (*Um*) was calculated from the muscle length data by differentiating the moving cubic regression. Absolute power output in W ($Nm.s^{-1}$) was divided by shortening velocity, *Um*, ($m.s^{-1}$) and resting (immediately pre-contraction) adductor cross sectional area, *ma*, (m^2) to give instantaneous force production per m^2 of adductor tissue, *Fspec*. This was corrected for the rotational movement of the valves which results in the force developed by the muscle acting in a different direction to the direction of movement of the muscle scar and the oblique position of the muscle within the shell.

$$Fspec = \frac{P}{Um \cdot ma} \cdot \left(Cos(\frac{Ag}{2})\right)^{-1} \cdot \left(\frac{Lm}{Lm_v}\right)^{-1}$$

Figure Legends

Fig. 1, Filming setup used for the recording of escape responses in *Aequipecten opercularis* and the co-ordinate system used to describe the position and orientation of the animal. Swim tank consisted of a glass tank (80 x 40 x 40 cm, length x width x height), fitted with a mirror above the scallop, at 45^{o} to the line of sight of the camera. A fixed co-ordinate system (x',y',z') described positions within the tank while the instantaneous co-ordinate system (x,y,z) described scallop orientation. The line of sight of the camera was the z' direction while the animal swum in the x' direction. The x,z plane was the commissural plane of the animal. The marked points on the scallop shell were used to improve digitising accuracy.

Fig. 2A. Shell gape against time during escape responses in *Aequipecten opercularis*, representative clap cycles at 5, 10 and 15^{o}C. The cycle at 5^{o}C is indicated by the solid line (—), at 10^{o}C by the dotted line (·····) and by the dashed line (– – –) at 15^{o}C. The form of the clap cycle changed with increasing temperature. The closing phase was completed more quickly with increasing temperature while the period of muscle lengthening remaining relatively unchanged. Traces were normalised - there were no significant differences in strain between "raw" cycle data for each temperature.

B) Net force experienced by the animal due to the thrust and drag forces during escape responses at 5, 10 and 15^{o}C. The cycle at 5^{o}C is indicated by the solid line (—), at 10^{o}C by the dotted line (·····) and by the dashed line (– – –) at 15^{o}C. Maximum thrust was higher at increased temperatures, with the point where drag exceeded thrust occurring earlier.

C) The effects of temperature on swimming velocity (*Ub*) during escape responses. Velocity against time plots are for representative animals at 5,10 and 15^{o}C. The cycle at 5^{o}C is indicated by the solid line (—), at 10^{o}C by the dotted line (·····) and by the dashed line (– – –) at 15^{o}C. Increases in temperature resulted in higher maximum speed (*Ubmax*) and higher residual speed at the end of the cycle. *Ubmax* was also attained earlier in the cycle as temperature increased.

Fig. 3. Calculated adductor muscle fibre shortening and lengthening velocities during escape responses. Representative cycles at 5°C (—), 10°C (·····) and 15°C (– –). While maximum shortening (negative values) and lengthening (positive) velocities were similar at all temperatures shortening was completed earlier (when fibre shortening and lengthing velocity=0 $Fl.s^{-1}$) with increasing temperature.

Fig 4 A). Workloops (*S* vs. F_{spec}) during escape responses. Representative cycles at 5°C (—), 10°C (·····) and 15°C (– –). Zero strain indicated that the adductor muscle was at its maximum length prior to the initiation of contraction. The area of the loop was proportional to the total work done during the cycle.

B) Force-velocity trajectories (*Um* vs. F_{spec}) during escape responses, representative cycles at 5°C (—), 10°C (·····) and 15°C (– –). Trajectories were similar at all temperatures though the duration of the shortening phase (negative values for muscle velocity) differed with temperature.

C) Muscle mass specific hydrodynamic power output (P_{spec}) during escape responses at 5°C (—), 10°C (·····) and 15°C (– –). Maximum values of P_{spec} (*Pmax*) were greater with increasing temperature but the "active" phase of positive power output was completed earlier. The negative power required to re-fill the mantle was small and similar at all test temperatures.

Fig A1. Morphological measurements taken from dissected *Aequipecten opercularis* and the angles and calculated lengths used in the calculations.

Table 1. Effects of acclimation temperature on whole-body and muscle performance measures during the first clap of escape responses in acclimated scallops (*Aequipecten opercularis*). Linear regressions of performance measures against temperature. Non-significant relationships ($p>0.05$) are not presented. (df=23 in all cases).

Performance type	Performance parameter	r^2	P
Whole body performance	Maximum swimming velocity, *Ubmax* ($m \cdot s^{-1}$)	0.673	0.002
	Mean cyclic swimming velocity, $\bar{U}b$ ($m \cdot s^{-1}$)	0.839	0.001
	Mean swimming velocity during jetting , $\bar{U}b_{jet}$ ($m \cdot s^{-1}$)	0.762	0.001
	Maximum acceleration, *Xbmax*, ($m \cdot s^{-2}$)	0.752	0.001
	Maximum net force, *Tmax*, (N)	0.741	0.001
Muscle performance	Maximum mass specific power output, *Pmax*, ($W \cdot kg^{-1}$)	N/S	
	Mean cyclic mass specific power output, $\bar{P}spec$, ($W \cdot kg^{-1}$)	0.471	0.02
	Maximum tension, *Fmax* ($kN \cdot m^{-2}$)	N/S	
	Mean tension, $\bar{F}spec$ ($kN \cdot m^{-2}$)	0.512	0.013
	Maximum fibre shortening velocity, *Ummax*, ($Fl \cdot s^{-1}$)	N/S	
	Mean fibre shortening velocity ($Fl \cdot s^{-1}$)	0.38	0.003
	Maximum fibre lengthening velocity ($Fl \cdot s^{-1}$)	N/S	
	Maximum flow ($kg \cdot s^{-1}$)	N/S	
	Maximum pressure (kPa)	N/S	
	Maximum jet velocity ($m \cdot s^{-1}$)	N/S	
	Maximum jet thrust (N)	N/S	

Table 2. Key whole-body and muscle performance parameters for animals acclimatised to 5, 10 and 15°C. Values given are means and standard errors for parameter for each group and the overall Q_{10} 5-15°C for each parameter.

Performance parameter	**Temperature (°C)**						
	5		**10**		**15**		
	Mean	SE	Mean	SE	Mean	SE	Q_{10} (5-15°C)
Maximum swimming velocity, *Ubmax* ($m \cdot s^{-1}$)	0.28	0.01	0.33	0.03	0.37	0.01	1.34
Mean cyclic swimming velocity, $\bar{U}b$ ($m \cdot s^{-1}$)	0.16	0.02	0.22	0.01	0.27	0.01	1.66
Mean swimming velocity during jetting , $\bar{U}b_{jet}$ ($m \cdot s^{-1}$)	0.08	0.01	0.11	0.05	0.16	0.02	2.01
Maximum fibre shortening velocity, *Ummax* ($Fl \cdot s^{-1}$)	-2.16	0.05	-1.78	0.26	-2.18	0.07	1.01
Maximum fibre lengthening velocity ($Fl \cdot s^{-1}$)	3.45	0.30	2.88	0.25	2.93	0.20	0.85
Mean fibre shortening velocity ($Fl \cdot s^{-1}$)	-0.51	0.04	-0.92	0.07	-1.05	0.08	2.04
Mean fibre lengthening velocity ($Fl \cdot s\text{-}^{1}$)	4.44	0.35	3.32	0.48	7.88	0.64	1.78
Maximum net force, *Tmax*, (N)	0.61	0.05	0.49	0.08	1.15	0.09	1.88
Maximum mass specific power output, *Pmax* ($W \cdot kg^{-1}$)	-139.16	40.02	-135.16	50.72	-221.64	33.65	1.59
Mean cyclic mass specific power output, $\bar{P}spec$ ($W \cdot kg^{-1}$)	-23.30	4.67	-11.66	3.78	-31.10	5.32	1.33

Table A1, Abbreviations of the parameters used in the model of scallop swimming applied in the present study. Where these scaled significantly with shell height (distance from hinge to forward tip of the animal's shell) the proportionality (b0) and scaling (b1) coefficients are provided. The subscripts $_t$ and $_b$ added to the above variables are used where appropriate to denote the top and bottom valves respectively. In all cases the expressions top and bottom refer to the animal as normally orientated and therefore do not conform to malacological convention. Similarly "forward" and "front" are taken to be the direction of movement during swimming.

	Scaling coefficients		
Parameter	**b0**	**b1**	**Abbreviation**
Angles (degrees)			
Gape angle			*Ag*
Internal angle from commissural plane to line joining hinge to muscle scar (*Lmh*)			*Ai*
Muscle extension angle (in x,y plane)			Am_{ext}
Muscle pull angle (from y direction)			*Ap*
Areas (m^2)			
Gape area			*ag*
Jet area	*0.00*	*0.89*	*ajet*
Adductor cross sectional area (resting)			*am*
Instantaneous adductor cross sectional area			am_{inst}
Shell plane area			*as*
Projected shell area			as_{proj}
Forces (kN or $kN.m^{-2}$)			
Force production of adductor muscle (kN)			*F*
Maximum tension ($kN \cdot m^{-2}$)			*Fmax*
Tension (muscle cross area specific force, $kN \cdot m^{-2}$)			F_{spec}
Mean cyclic tension ($kN \cdot m^{-2}$)			$\bar{F}_{spec}$
Lengths (m)			
Shell circumference			*Lc*
Gape			*Lg*
Gape at digitising points			Lg_{points}
Hinge length	0.03	1.70	*Lh*
Hinge arc			Lh_{arc}
Hinge to centre of mass of valve			*Lhcom*
Adductor length (taking into account lateral and anterior-posterior obliqueness)			*Lm*
Anterior-posterior displacement of muscle scars			Lm_{anti}
Muscle scar to front lip of shell			*Lmf*
Muscle scar to hinge			*Lmh*
Adductor length (corrected for lateral offset)			Lm_{lat}

Lateral displacement of muscle scars in x direction	0.09	0.87	*Lmm*
Maximum adductor length			*Lmmax*
Adductor length (assuming vertical)			Lm_v
Shell depth	0.55	0.89	*Lsd*
Shell height			*Lsh*
Hinge to digitising points			Lsh_{points}
Projected shell height			Lsh_{proj}
Shell length	1.84	0.86	*Lsl*
Masses (kg)			
Body mass	0.00	2.78	*Mb*
Virtual body mass			$Mb_{virtual}$
Adductor mass	0.00	5.55	*Mm*
Mass upper valve	0.00	2.03	*Ms*
Power outputs (W or $W \cdot kg^{-1}$)			
Power (W)			*P*
Mass specific power ($W \cdot kg^{-1}$)			P_{spec}
Maximum mass specific power output ($W \cdot kg^{-1}$)			*Pmax*
Mean cyclic mass specific power output ($W \cdot kg^{-1}$)			$\bar{P}spec$
Thrusts (N)			
Net force on body, as calculated from acceleration			*T*
Maximum net force (thrust > drag)			*Tmax*
Minimum net force (thrust < drag)			*Tmin*
Velocities ($m.s^{-1}$)			
Swimming velocity			*Ub*
Maximum swimming velocity			*Ubmax*
Mean cyclic swimming velocity			$\bar{U}b$
Mean swimming velocity during jetting			$\bar{U}b_{jet}$
Intake velocity			Uin
Jet velocity			*Ujet*
Fibre shortening velocity ($m \cdot s^{-1}$)			*Um*
Fibre shortening velocity (fibre length specific), ($Fl \cdot s^{-1}$)			$\hat{U}m$
Maximum fibre shortening velocity (fibre length specific) ($Fl \cdot s^{-1}$)			$\hat{U}mmax$
Volumes (m^3)			
Jet cavity volume			*vc*
Shell volume			*vs*
Accelerations ($m \cdot s^{-2}$)			
Maximum whole body acceleration (tangential)			*Xbmax*
Whole body acceleration (tangential)			Xb_{tang}
Whole body acceleration (total)			Xb_{total}
Maximum whole body acceleration (total)			$Xb_{total}max$
Miscellaneous			
Flow ($m^3 \cdot s^{-1}$)			*f*
Strain (*Lm*/*Lmmax*)			*S*
Kinematic viscosity ($m^2 \cdot s$)			*u*
Density of seawater ($kg \cdot m^{-3}$)			ρ

Fig 1

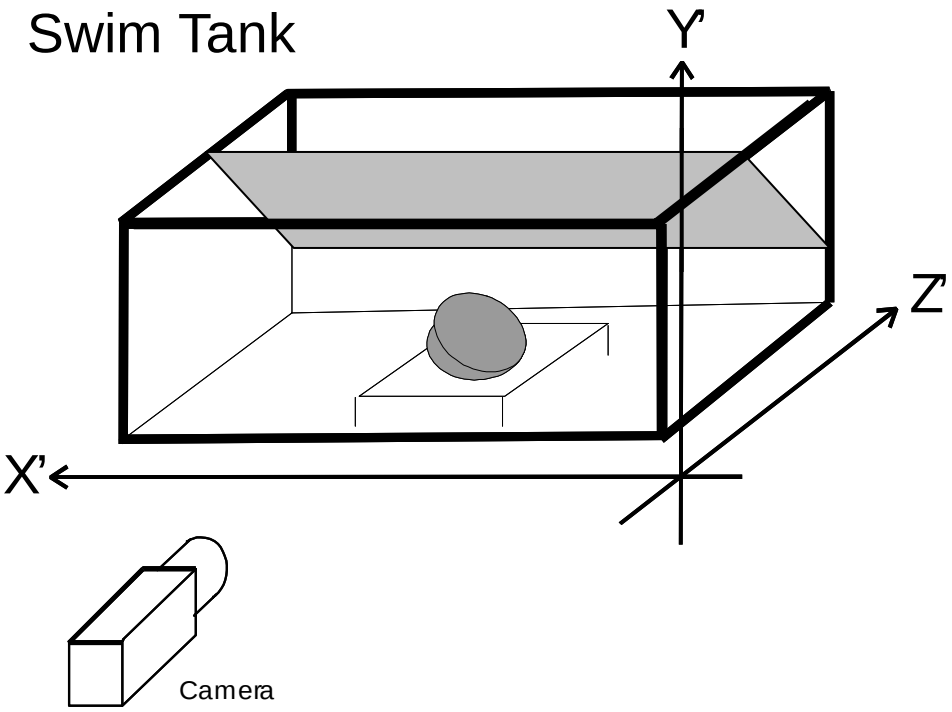

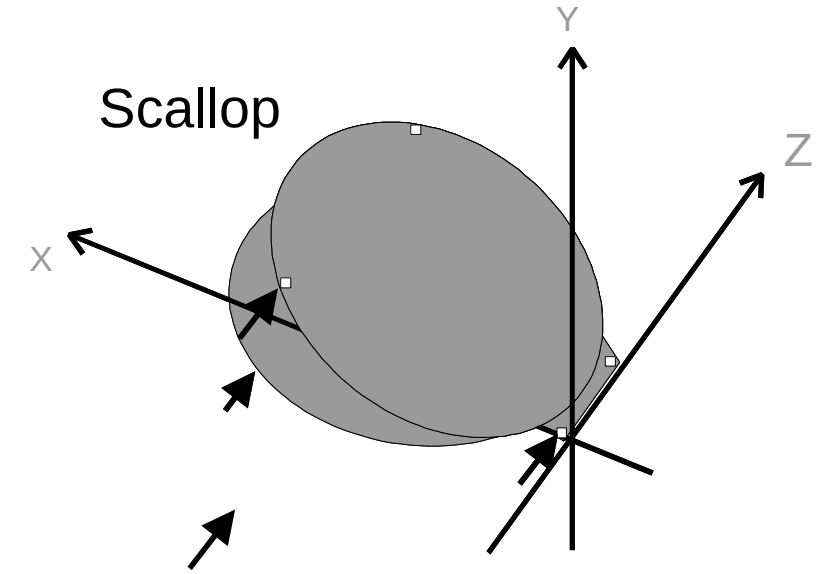

Indicates position of digitising points. These were repeated on the opposite side

Fig 2

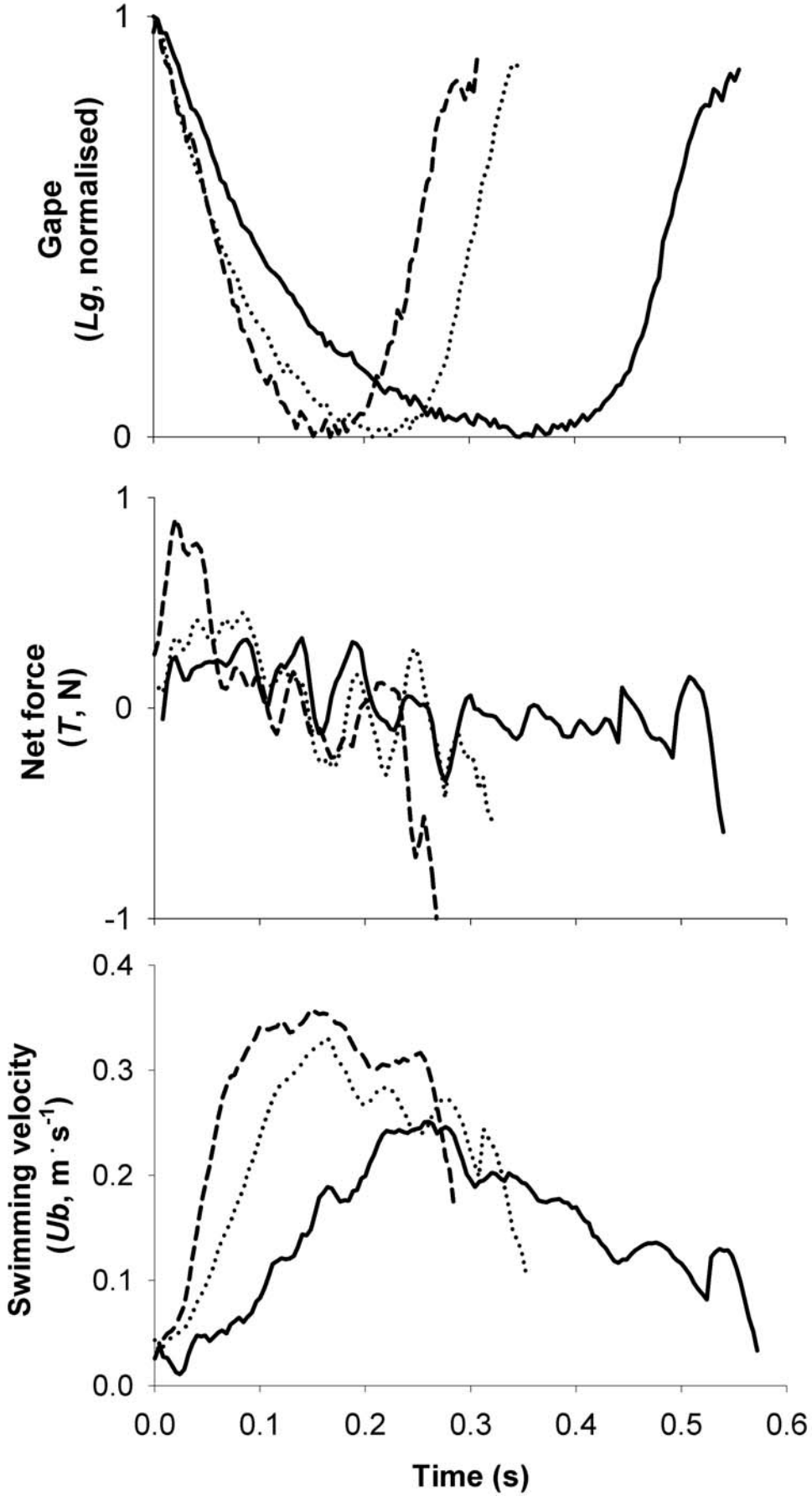
Gape
(Lg, normalised)
1
0
Net force
(T, N)
1
0
-1
Swimming velocity
(Ub, m · s-1)
0.4
0.3
0.2
0.1
0.0
0.0
0.1
0.2
0.3
0.4
0.5
0.6
Time (s)

Fig 3

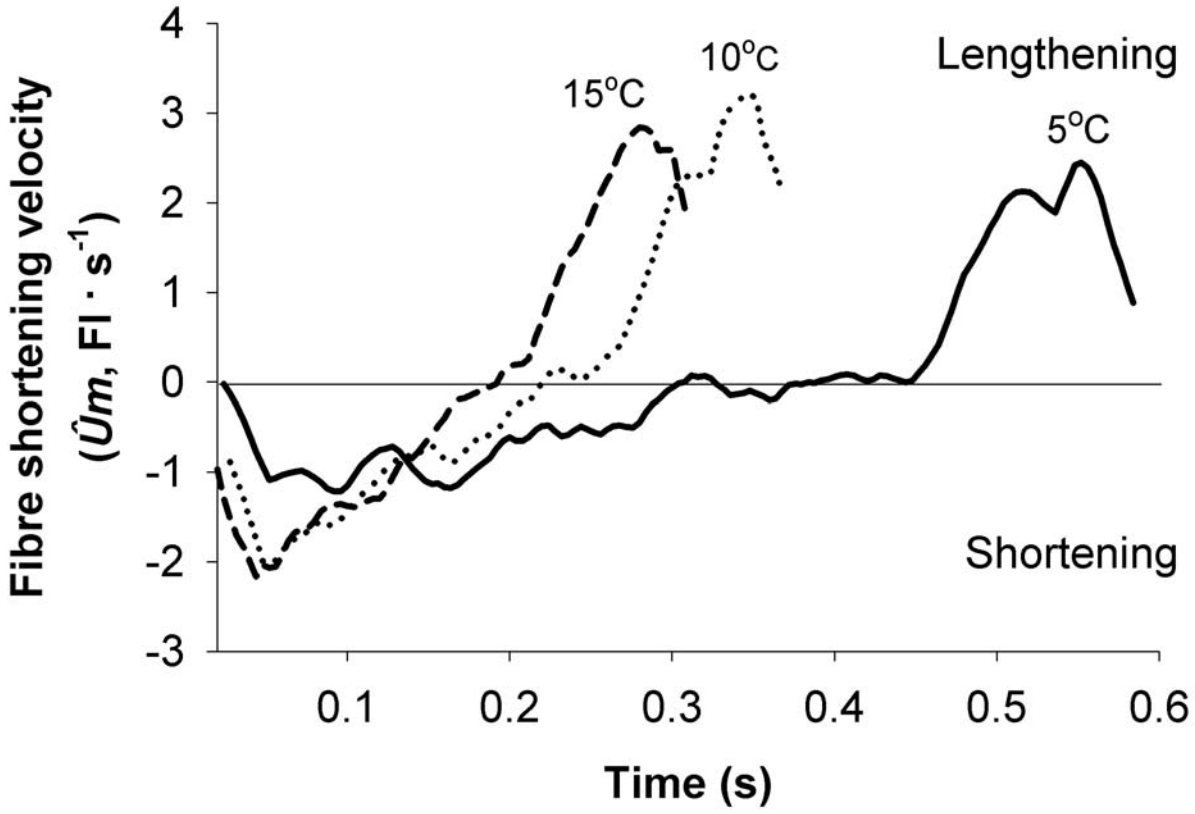
Fibre shortening velocity
(Ûm, Fl · s-1)
4
3
2
1
0
-1
-2
-3
0.1
0.2
0.3
0.4
0.5
0.6
Time (s)
15°C
10°C
5°C
Lengthening
Shortening

Fig4A

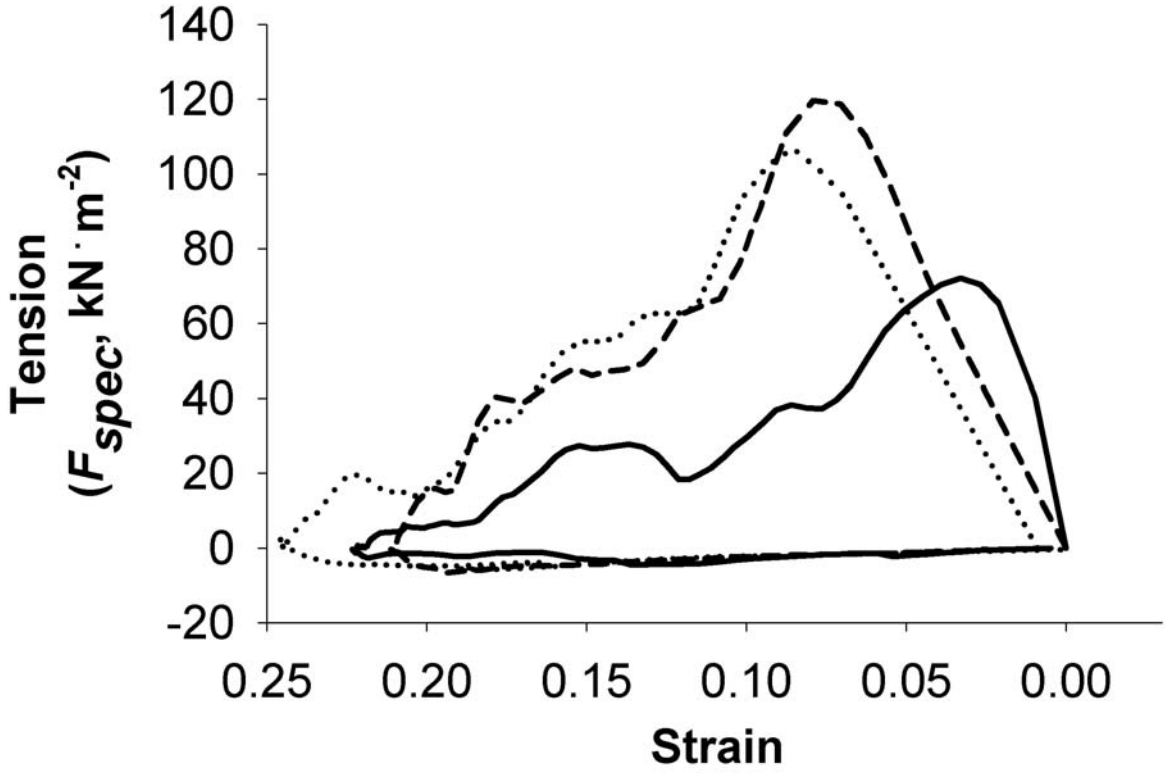
140
120
100
80
60
40
20
0
-20
Tension
(F_{spec}, kN · m^{-2})
0.25
0.20
0.15
0.10
0.05
0.00
Strain

Fig

4B

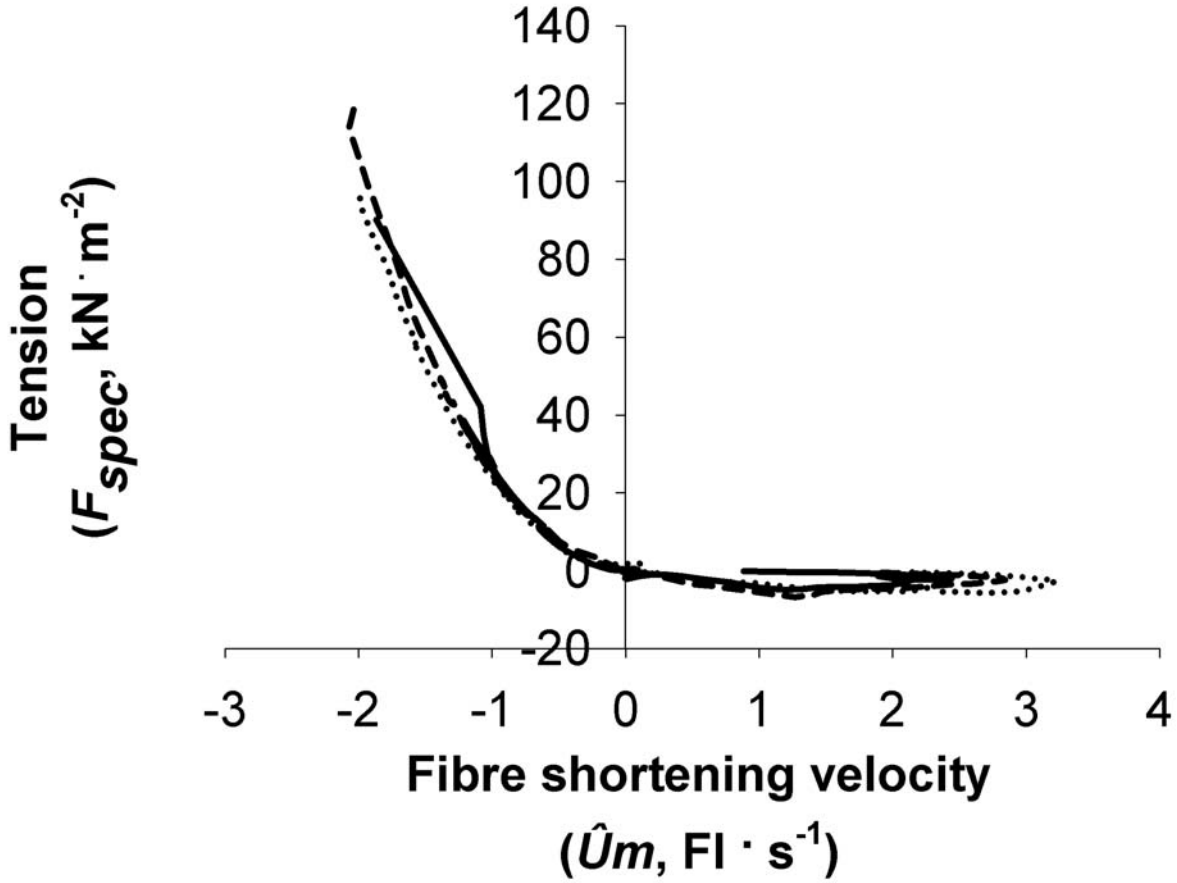
140
120
100
80
60
40
20
0
-20
-3
-2
-1
0
1
2
3
4
Tension
(F_{spec}, kN · m^{-2})
Fibre shortening velocity
($\hat{U}m$, Fl · s^{-1})

Fig 4C

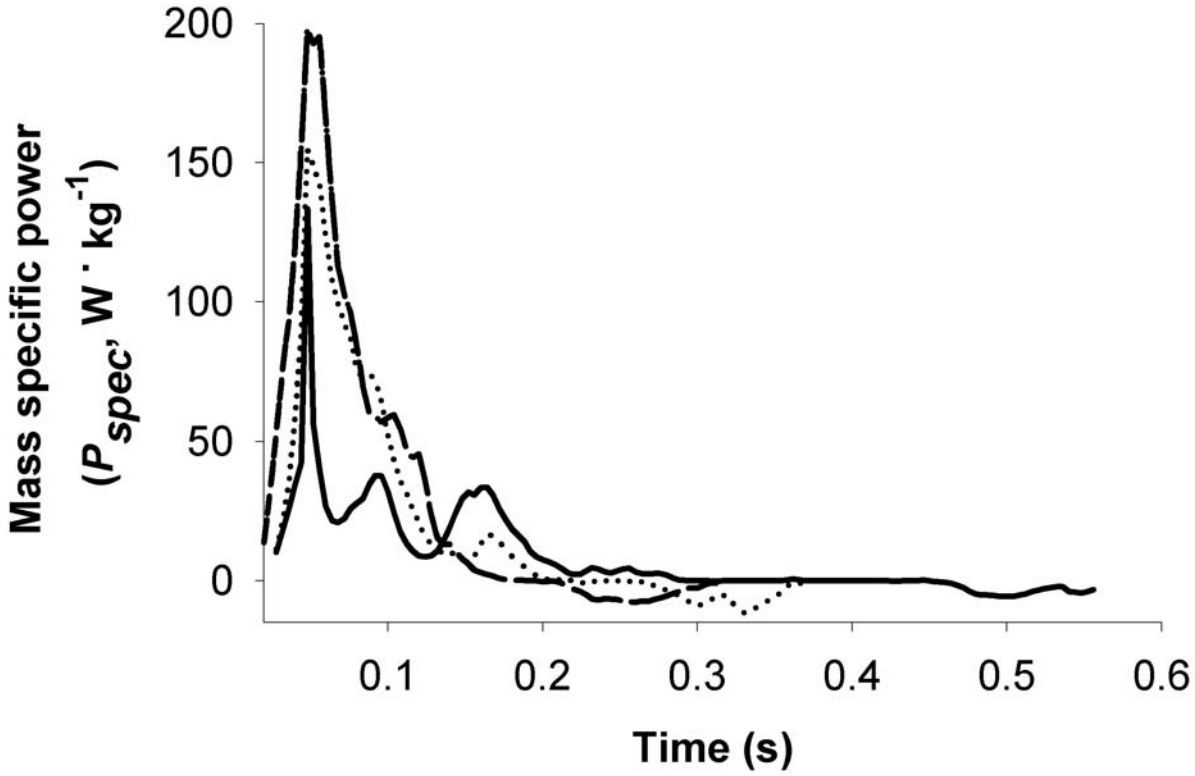
Mass specific power
(P_{spec}, W · kg^{-1})
200
150
100
50
0
0.1
0.2
0.3
0.4
0.5
0.6
Time (s)

Fig A1, Side view, anatomical dimensions used in the calculations

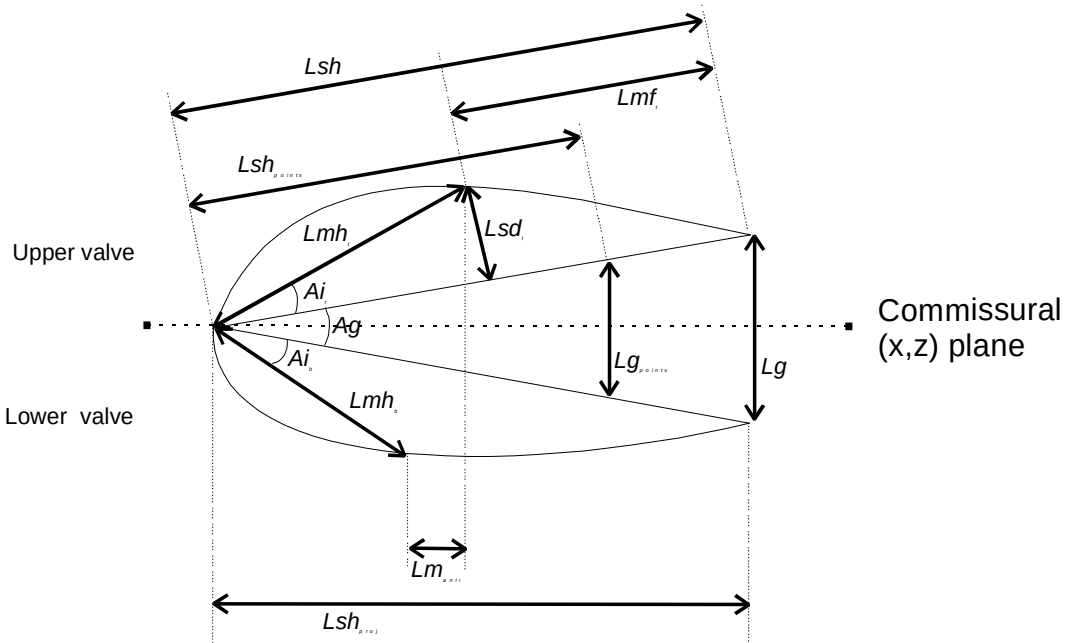

Fig A2, Top view